# Exhumed conduit records magma ascent and drain-back during a Strombolian eruption at Tongariro volcano, New Zealand



**Fabian B. Wadsworth[1], Ben M. Kennedy[2], Michael J. Branney[3], Felix W. von Aulock[4], Yan Lavallée[4], Amaya Menendez[5]**

*1 Earth and Environmental Science, University of Munich, Theresienstr. 41, 80333 Munich, Germany.*
*2 Geological Sciences, University of Canterbury, Private Bag 4800, Christchurch 8140, New Zealand.*
*3 Department of Geology, University of Leicester, Leicester, LE1 7RH, United Kingdom.*
*4 Dept of Earth, Ocean and Ecological Sciences, University of Liverpool, Liverpool, U.K.*
*5 Ocean and Earth Science, National Oceanography Centre, Southampton, SO14 3ZH, U.K.*

**Field evidence from a basaltic-andesite dyke preserved in the eroded wall of a scoria cone at Red Crater, Tongariro volcano, New Zealand records a history of up-conduit magma flow during a Strombolian eruption, subsequent drain-back and final cessation of flow. The dyke intrudes pre-Strombolian andesite lavas, and the overlying proximal basaltic-andesite scoria deposits associated with contemporaneous lavas, which are, in turn overlain by laminated lapilli-tuff and large blocks. Textural and kinematic evidence of ductile shear recorded in basaltic andesite at the dyke margins records magma deformation imposed by bypassing movement of magma up the centre of the conduit during the eruption, whereas the basaltic andesite occupying the central part of the lowermost exposures of the dyke preserves ductile flow-folds with the opposite (down-flow) shear-sense. The evidence indicates that the downward magma flow followed the eruption, and this draining left the central part of the dyke empty (unfilled) at uppermost levels. We discuss the kinematic constraints in the context of the criteria for up-flow of mafic magma, and present the factors most likely to result in a final drain-back event. With reference to experimental and numerical work we propose a draining model for the end of this eruption, and that magmatic drain-back may feature commonly during closing stages of Strombolian eruptions at mafic volcanoes. Drain-back which leaves large cavities in a volcanic edifice could result in hazardous structural instabilities.**

**Introduction: down-flow in conduits**

Conduit processes involving downward motion of magma relative to the walls that have been invoked at volcanoes include local down-flow during convection (e.g. Genareau et al. 2010; Witter et al. 2004), exchange flow (e.g. Palma et al. 2011), wholesale conduit-filling down-flow (Lefebvre et al., 2012; Witham and Llewellin 2006), and downward motion at the walls of rising conduit-filling Taylor bubbles (Llewellin et al. 2012). These examples are driven by different fluid mechanics and act over contrasting timescales, but all have preservation potential in the form of a textural record so long as the motion is accompanied by solidification or accretion of magma against conduit margins due to cooling and/or crystallisation.

Magma draining is manifested in cycles of changing lava-lake surface level, such as at Pu'u'O'o (Garcia et al. 2000; Heliker and Wright 1991) and Kilauea Iki (Stovall et al. 2009) in Hawaii, Villarrica in Chile (Witter et al. 2004), Erta Ale in Ethiopia (Bizouard et al. 1980; Harris et al. 2005), Nyiragongo in the Democratic Republic of Congo (Demant et al. 1994), Stromboli in Italy (Giberti et al. 1992; Laiolo and Cigolini 2006) and Mt Erebus in Antarctica (Dibble et al. 1984; Oppenheimer and Kyle 2008). It has been inferred from geophysical signals, such as microgravity anomalies at Izu-Oshima volcano (Watanabe et al. 1998). In these examples, down-flow of magma was proposed as the most tenable explanation for the observations, which range from geophysical to petrological in nature. However, the direct kinematic record of down-flow in conduits is rarely exposed or reported.

Repeated cycles of draining of basaltic magma from a lava-lake at Kilauea Iki are recorded texturally by accreted veneers of basalt that preserve evidence for downward ductile deformation (Stovall et al. 2009). In this example, repeated cycles of lava-lake filling and draining that drove the formation of these features with plastering, cooling and preservation of the veneers occurred over short timescales. Cyclicity of draining and re-filling at lava lakes may be driven by outgassing-induced pressure instabilities at a conduit reference depth such that densification of magma during passive degassing leads to pressure build-up at the conduit base (Witham and Llewellin 2006).

At Higby Mountain, Connecticut, up-flow followed by down-flow of low-viscosity magma was invoked to explain bimodally trending vesicle strain ellipses in a basaltic (camptonite) dyke (Philpotts and Philpotts 2007). The textures recording up-flow occur near the margin of the dyke rock, whereas the down-flow textures are found toward the dyke axis. Upward flow textures were progressively quenched in prior to down-flow at the dyke axis. In this case, there is insufficient evidence to deduce the driving mechanism for the change from upward to downward flow. Conduit textural evidence and observations of the eruption AD 1809 eruption at Etna volcano support inference of a late-stage drain-back event during which magma was withdrawn from the feeder system (Geshi and Neri 2014).

Accounts of drainback during the AD 1809 Etna eruption are consistent with analogue experiments and simple models of pressure-driven conduit flow that have helped elucidate down-flow mechanisms. Experimentally verified down-flow mechanisms include pressure instabilities at a reference depth due to outgassing through lava lakes (Witham and Llewellin 2006; Witham et al. 2006), exchange flow driven by evolving density contrasts between more and less degassed magma (Palma et al. 2011) and local down-flow in the falling film of Taylor bubbles (Llewellin et al. 2012) or down-flow of the melt phase associated with any two-phase flow in which the gas and liquid are not strongly coupled (e.g. Jaupart and Vergniolle 1989).

This paper presents an exposed rare example of a mafic conduit with textural evidence for up-flow and down-flow phases of activity within the context of a Strombolian eruption that is recorded by erupted products. We then use the example to discuss different causes of down-conduit magma flow.

## Red Crater volcano stratigraphy

An exceptionally well-preserved mafic conduit is exposed at Red Crater volcano, part of Tongariro Volcanic Centre, which lies within the dominantly andesitic SSW end of Taupo Volcanic Zone, New Zealand (Cole et al. 1983). The dominant regional fault trend is NNE-SSW, similar to the boundaries of the Taupo Volcanic Zone (Fig. 1; Nairn et al. 1998). At Red Crater volcano, the Emerald Lake craters and Ngauruhoe volcano align along a similar NNE-SSW trend (Hobden 1997; Hobden et al. 1999), and may be linked by dykes of similar orientation at depth. At Red Crater volcano, the eruption evolved from andesite to basaltic-andesite compositions, and the basaltic-andesite eruptions produced a proximal scoria cone (Fig. 2). The site stratigraphy can be divided into pre-Red Crater deposits, the Red Crater volcano andesite lavas and the Red Crater volcano basaltic-andesites including the scoria cone (Fig. 3).

The pre-Red Crater Tongariro Trig andesite, a 65-110 ka (Hobden 1997) porphyritic block lava, ≥30 m thick and dipping 30° north, underlies all proximal Red Crater volcano deposits (Fig. 2) and pre-dates the last glaciation (14 ka; McArthur & Shepherd 1990). The Red Crater volcano andesite lavas are the most voluminous products from this eruptive centre (Hobden 1997; Stevens 2002) and underlie the Red Crater basaltic-andesites which include lavas, the proximal scoria deposits and fine grained distal tephra (Fig. 2; Moebis et al. 2011).

The basaltic-andesite beds in the lower sections of the scoria cone are interbedded with layers of lava with relict spatter deposits that grade laterally into less dense, granular scoria beds (Fig. 2-3), indicating that in these lower parts of the cone, the scoria locally agglutinated upon deposition. Where agglutination is evident, scoria clasts in the lower part of the scoria cone are flattened parallel to bedding (Fig. 3). Clasts in the upper parts of the scoria cone are more equant, porous and angular, with no evidence for agglutination or flattening (Fig. 3). The basaltic-andesite lavas outside the scoria cone were emplaced in basins to the north and south of the vent and are locally inter-fingered with scoria

(Bardsley, 2004), suggesting that they were dominantly spatter-fed from zones of agglutination and coalescence. Distal (~1-10 km) fall deposits have been correlated with eruptions from Red Crater volcano using a diagnostic range of $K_2O$/FeO and $SiO_2$ to differentiate them from other Tongariro Volcanic centre or Ruapehu volcano deposits, leading to discrimination of 16 discrete eruptive events in the last 300 years (Moebis et al., 2011). The underlying Red Crater andesite lavas predate these tephra by an unknown amount of time.

Overlying the scoria are finely laminated beds of tuff and lapilli-tuff, ranging in thickness from a few millimeters to tens of centimeters (Fig. 2). The grainsize of the laminated tuff ranges from fine to coarse ash. The lapilli-tuffs range from massive to low-angle cross-stratified, and locally have impact-sags beneath blocks up to 50 cm. Large, meter-sized juvenile blocks occur on the cone surface. The scoria deposits all contain high, but variable proportions of hydrothermally altered lithic fragments (Menendez, 2014).

**Dykes in the Red Crater scoria cone: eruptive conduits**

Several dykes cross-cut the volcano; the smallest are irregular in geometry and strike. A NNE-striking dyke exposed in both north and south crater walls intrudes the upper autobreccia of the Tongariro Trig andesite and the lower part of the Red Crater scoria cone (Fig. 2 & 4). Above the andesite, it widens and splay laterally into the scoria deposits, which are locally altered within ≤2.5 m-wide contact aureoles parallel to the dyke margins. The aureoles are vertically pervasively fractured perpendicular to the strike of the dyke (Fig. 4). Within the contact aureoles, the scoria clasts are fused to the dyke margins, whereas away from the dyke the scoria bombs and lapilli remain loose and poorly consolidated.

On the south side of Red Crater the dyke dips ~45º and is 5 m wide where it intrudes the brecciated Tongariro Trig andesite, and it becomes vertical and reaches a thickness of ≤11 m where it intrudes the scoria deposits. An open, central cavity, 8 m wide, occupies the central part of the dyke. The dyke rock is divided texturally into a marginal facies and central facies, separated by locally sharp boundaries marked by abrupt changes in phenocryst content, truncated flow-foliation, vesicle size distribution, and vesicularity (Fig. 5).

The width of the marginal facies varies from 0.7-1.2 m in the lower part of the dyke to 0.3 m near the top of the dyke (Fig. 1b). A 1-2 cm–wide microcrystalline chilled rim lies against the contact with the scoria host. The phenocryst assemblage and relative abundances do not obviously change between facies, but the sizes of phenocrysts increase from ≤0.5 mm at the outer contact to 1.5-3 mm across ~ 1 m towards the interior (Fig. 6), and the size of vesicles increases from <3 mm near the outer contact to ~5-15 mm toward the interior, and vesicles also become prolate and irregular in shape 1 m in from the outer contact. At the lower part of the dyke, the outer contact is generally straight and sharp, but with local mm-scale projections into interstices between scoria clasts of the host deposit.

Cooling joints spaced <0.5 m are ubiquitous in the dyke rock perpendicular to the margin. The marginal facies has a flow-foliated microlite-rich groundmass. On the east side of the dyke, the flow foliation dips 25-31° to the northwest, and on the west side it dips 20-25° to the west (Fig. 4). Where the dyke intrudes the Red Crater scoria, the foliation steepens to 85-90°. It is sub-parallel to the dyke margins in the lower part of the dyke and parallel in the upper part (Fig. 7). Where the dyke intrudes the Tongariro Trig andesite lava autobreccia, the west marginal facies is autobrecciated (Fig. 4).

The marginal facies exhibits a 0.3 m-wide shear-zone characterised by a S-C fabric defined by aligned microlites and vesicles (Fig. 4). The shear-zone is parallel to the dyke margin, and contains a foliation-parallel lineation defined by WNW-trending 5–15 mm irregular vesicles that plunge ~45º in the lower parts of the dyke, and steepen to vertical in the upper part (Fig. 7).

The inner contact of the marginal facies is locally sharp and defined by a prominent lineation, and an increase in phenocryst abundance towards the central facies. The marginal facies contact with the central cavity has close-spaced prismatic cooling joints.

The central facies is 3.5 m wide in the lower part of the dyke, and is absent in the upper part. The eastern contact between the central facies and the marginal facies is locally asymmetrically folded, with folds verging down dip to the northwest (Fig. 5). In the lowermost part of the dyke vesicle deformation in the central facies is greatest near the outer contact with the marginal facies, and lowest at the centre of the dyke, where the flow-foliation also is less well-developed. At the dyke axis, the flow-foliation is arcuate and discontinuous (Fig. 4) whereas near the outer margin of the central zone it is margin-parallel and continuous. In contrast, the upper part of the central zone has an irregular, subhorizontal flow foliation with oblate, variably dipping large vesicles (Fig. 4). Rare scoria clasts with distinct outlines are embedded within the uppermost part of the central zone.

The central, upward-gaping cavity is ~8 m wide above the central zone and thins to the south along the strike of the, to a lateral termination within the host Red Crater scoria. The walls of the central cavity are irregular with ~10 cm wide horizontal and subhorizontal in-stepping benches (Fig. 4). The upper part of the interior wall has polygonal prismatic cooling joints perpendicular to the cavity wall whereas the lower part exhibits vertical flow foliation and undulose flow features that resemble pahoehoe toes (0.1-0.2 m), jointed in cross section.

The central cavity of the dyke contains well laminated tuffs, dipping towards the cone centre. These tuffs are composed of coarse to fine ash and appear stratigraphically consistent with the units of interbedded tuffs and lapilli-tuffs that overlie the scoria deposits elsewhere (Fig 2) and clearly relate to late stages of the Red Crater eruption.

## Interpretation

The dyke in the south wall of the proximal scoria cone at Red Crater volcano was emplaced after most or all of the scoria was deposited but before the deposition of the overlying fine-grained deposits

182 which also appear inside the drained interior of the dyke. This dyke erupted at the surface, as recorded
183 by the ejected scoria clasts that fell back into the dyke to become embedded in the still-viscous magma
184 (Fig. 4) as proposed elsewhere (Cimarelli et al. 2010; Lautze and Houghton 2005; Lautze and
185 Houghton 2007).

186 The laminated ash within the open dyke records the last phreatomagmatic phase of the
187 eruption. These relations indicate that at least some of the Strombolian activity at Red Crater was fed
188 by the dyke. Parts of the dyke intrude lower parts of the Strombolian scoria, so the intruded parts of
189 the scoria cone had accumulated prior to emplacement of this uppermost part of the dyke.

190 Early rise of magma in this uppermost dyke segment was recorded in the marginal zones of
191 the dyke, and later down-flow is recorded by textures in the dyke centre. A similar up- then down-flow
192 history was inferred from by vesicle and AMS patterns in a camptonite dyke in the USA that has no
193 associated eruption products (Philpotts and Philpotts 2007). Up-flow is first recorded by the micro-
194 crystalline and jointed margin in which phenocrysts are aligned parallel to or imbricated against the
195 marginal contact, suggesting that the vanguard magma was plastered to the walls of the dyke and
196 rapidly cooled *in situ* before or while being bypassed by additional ascending magma which widened
197 the dyke. The small-scale bulging of the dyke at the interface between the two wall-rock lithologies,
198 the underlying lava and the overlying scoria deposits, may indicate the effects of differential host
199 densities or elastic properties (Taisne and Jaupart 2009) on progressive dyke emplacement such that
200 widening occurs in the least well-consolidated deposit, here the scoria. Alternatively, explosivity
201 associated with Strombolian activity may result in dyke conduit flaring (Geshi et al. 2010; Keating et
202 al. 2008). Progressive up-flow during incipient cooling probably led to the development of a lateral
203 rheological gradient which continued to evolve through time as cooling of the melt and eventual
204 crystallisation occurred during the magma's progressive outside-inward solidification. Such a process
205 is driven by increasing melt viscosity and crystallisation and evidenced by an increasing microlite
206 content and increasing mean microlite size away from the dyke margin. Increases in magma viscosity
207 close to an in-stepping margin are consistent with the C-S fabrics observed ~0.5 m from the marginal
208 contact. Such fabrics typically reflect strain instability and localisation on shear planes when lateral
209 rheological gradients are steep or shear rates are high (Clemente et al. 2007). Progressive in-stepping
210 of the solidification front proceeded sufficiently rapidly to preserve these up-flow textures. The up-
211 flow textural features, i.e. the C-S fabrics and the flow foliation follow the marginal contacts. For
212 example, along the eastern side of the dyke, the flow foliation changes from 41-47° where the dyke
213 margin is 45° at lower levels to near vertical in upper parts of the dyke where the dyke margin is also
214 near vertical (Fig. 7).

215 A sharp planar contact between the up-flow marginal facies and the down-flow central facies
216 is inferred to have developed at the onset of down-flow Locally, parts of the marginal facies, past
217 which magma drained back, were still deformable in a ductile manner such that the contact between
218 the two facies is folded, a typical shear-mingling deformation pattern when fluids of slightly different

rheology flow past one another (Miles 1959). These flow-folds coupled with the downward plunging elongate vesicles in the central facies are diagnostic of relative flow directions (Fig. 4; Fig. 5). The frozen textures in dykes rarely preserve the structure of the flow, however, and more likely were progressively accumulated. Therefore, we do not attempt to quantify the draining rates from the vesicles found in the central portion of the dyke at Red Crater volcano. The vesicle textures are oblique to the margins of the central facies such that they plunge toward the centre of the crater. Similarly, weakly developed flow foliation at the top of the central facies dips toward the centre of the crater parallel to the frozen top of the central facies (Fig. 4).

Assuming that the dyke was once full of magma to the tip, the maximum down-flow distance was 40 m. However, we acknowledge that some of that space could have been produced by eruption of material and not all necessarily was drained. Following removal of the central magma from the upper part of the dyke, the walls, then still ductile, locally slumped and collapsed (Fig. 1b), and the down-flow is recorded by the pahoehoe-style flow toes on the inner walls of the dyke's central cavity. Finally, cooling joints are developed everywhere on the exposed inward-facing interior walls of the marginal dyke-rock, and indicate that the magma had accreted to the dyke walls at high temperature and that the draining then caused marked chilling by exposure to the air within the open-vent (Fig. 4).

The observation that the up-flow is recorded by near-vertical kinematic indicators whereas downward flow is recorded by oblique indicators that plunge toward the crater centre (Fig. 7) suggests that draining occurred both downward and also toward a possible feeder at the crater centre, which is now not preserved at the surface.

## Discussion

### *Mechanisms for downward flow in conduits*

Mechanisms that might account for downward flow of magma in a conduit include some that act on the lengthscale of elements within the conduit, such as bubbles, and those that act on longer lengthscales such as the conduit length.

First, on small lengthscales, a film of magma will flow downward around a rising slug of gas ('Taylor bubble') and the film has a predictable thickness and velocity for the conduit geometry and magma rheology (Llewellin et al. 2012). Also, when a Taylor bubble reaches a magma free surface at the top of a conduit and bursts, remaining melt-film material may fall down into the conduit (Gonnermann and Manga 2007). These phenomena are transient and in order for a record of them to be preserved cooling timescales in the melt film must have been close to or less than the rise timescale of the bubble.

Second, on larger scales, convection or exchange-flow of initially density-stratified magma can occur at in magma-filled conduits (Palma et al. 2011; Stevenson and Blake 1998). The steady state

organisation of the down-flowing and up-flowing components of the conduit have been experimentally investigated in cylindrical geometry (Arakeri et al. 2000; Debacq et al. 2003; Huppert and Hallworth 2007; Palma et al. 2011) and depend primarily on that geometry and the ratio of the physical properties of the two fluids. This behaviour has been invoked in the conduit of Villarrica volcano (Witter et al., 2004) and is implicit in the modelling of explosive basaltic eruptions proposed by Parfitt and Wilson (1995) and Parfitt (2004). Persistent outgassing of a stagnant column of magma is a special case of exchange flow in which the rising poorly coupled gas phase can escape freely and the remnant dense magma flows downward, relatively and repeatedly. Textural evidence for exchange flow could feasibly be preserved but such flow is not likely to leave behind a large cavity at the top of the conduit.

At the lengthscale of the conduit itself, pressure perturbations due to outgassing through an overlying lava lake can induce pressure increases at the interface between the conduit and a reservoir such that wholesale down-flow of the conduit magma is induced (Witham and Llewellin 2006). This is contingent on the lava lake radius being large compared with the conduit radius. There is no evidence for lava lake activity at Red Crater volcano and the widening of the conduit at the uppermost section is small. For these reasons, we do not invoke this mechanism for our magma migration scenario. Similar arguments could invoke a drop in pressure in the magma chamber by another mechanism to a point where it is lower than the pressure at the base of the conduit, which would result in backflow until equilibrium pressure is re-established.

Finally, downward flow of magma can ensue locally if magma is erupted at another point in a dyke (Lefebvre et al. 2012). This concept is conceptually illustrated in schematics of eruptions at Mount Etna; for example in drawings of the dyke system feeding the AD 1809 event (Geshi and Neri 2014). At Red Crater, the scoria cone's geometry shows that it was built from a near-point source, however, as the eruption progressed, the feeder dyke emplaced laterally into an increasing thickness of scoria deposits. Therefore, the dyke geometry is a shallow, local feature such that an eruption and removal of material from the along-strike crater-central portion of the dyke (not preserved) may have provided space for the magma at the lateral terminations of the dyke to move back toward the dyke centre. This lateral motion of magma from the dyke tips in the scoria walls toward the dyke centre would produce apparent down-flow textures on the walls of the dyke and a central cavity and the observed oblique sense of the down-flow kinematics (Fig. 7). This part of the dyke overlying the conduit itself has been subsequently removed by late-stage explosive activity and is no longer preserved.

While there are varied scenarios in which down-flow could be envisaged at mafic volcanoes, some of which are described here, local reorganisation of magma in a dyke that is erupting at a single point remains the least explored and is how we interpret this exposed dyke segment to have formed. We envisage that the magma in the dyke re-organised following a late eruptive event at one location where material was removed, possibly in the waning stages of eruption such that fresh material did not

replenish the dyke's volume rapidly. We use these observations to suggest that organisation of up-flow and down-flow regimes in dykes by any of the mechanisms described, is probably common and deserves further consideration because it may affect or control local flow dynamics and eruptions.

### *Timing of events in the basaltic-andesite phase at Red Crater volcano*

The dyke records upward flow of magma, and recycling of scoria clasts, attesting to its role in supplying magma for the scoria eruptions. During this phase perched magma within this and/or similar adjoining dykes fed fire fountains, resultant spatter-fed lavas and sustained Strombolian activity which became progressively centralised to the scoria cone's primary vent. As the cone built, the dyke continued to intrude upward into the scoria pile. The strike of the dyke at the shallowest level of exposure in the cone wall need not be the orientation at depth. Indeed, the Emerald Lake craters trend is ~30-45° oblique to the dyke strike and yet they are probably related to the same subsurface magma system. The dyke records subsequent downward flow of magma, and possibly lateral down-flow towards the central vent. The stratigraphic position of the dyke tip at the top of the scoria pile indicates that draining coincided with waning and eventual cessation of scoria-producing eruptions.

Following the draining of the dyke, eruptive activity changed from dominantly magmatic to dominantly hydrothermal, during which a series of late explosion craters exhumed the present cross-section of the dyke, and formed the present morphology of the crater and the NE-SW-trending chain of Emerald Lake craters (Fig. 1). The small-volume explosions fragmented and ejected rocks from the shallow hydrothermal system (Menendez 2014) producing laminated lapilli-tuff in the dyke and as bedded lapilli-tuff containing block impact sags, which reach thicknesses of 9 m on the flanks of the proximal vent (Fig. 3).

It is possible that magma-draining events such as that seen in the Red Crater dyke led to depressurisation and structural instabilities at the conduit walls that then led to the later phreatic explosivity. In addition, the slumping inward of the dyke arms is a testament to the gravitational instability of an empty cavity inside a scoria cone. Draining of a dyke may produce unstable cavities that induce avalanching of the crater walls into open vents and rapidly change eruption style and hazards around the vent. The outer flanks of volcanic edifices may also be subject to weakening through intrusion or draining, and such weakening is inferred to have preceded and facilitated the 2012 explosive eruption at Te Maari (Fitzgerald et al. 2014).

## Conclusions

Textures and kinematic indicators in a basaltic-andesite dyke within Red Crater, New Zealand, indicate initial magma up-flow in accreted marginal zones, followed by magma drain-down in the central zone, leaving an open, gaping conduit ~10 m below the cone summit. Both the magma rise and

subsequent drain back can be tied to the Strombolian phase of the Red Crater eruption, by the presence of scoria lapilli that dropped into the draining dyke and welded into the dyke rock, by pervasive cooling joints on the inward-facing partly drained dyke walls, and subsequent filling by late-stage phreatic products. A variety of mechanisms to account for the drain-back features is considered and a late-stage local shallow draining of magma toward the scoria cone centre is invoked to explain the stratigraphy.

## Acknowledgments

We thank James D. L. White for a critical reading of the manuscript, Sonia Calvari for editorial handling, Marco Neri, Nabuo Geshi and Ed Llewellin for reviews of our work and Paul Ashwell, James Cowlyn, and Simon Bloomberg for field assistance. We are grateful to the New Zealand Department of Conservation for field access and sampling permission. B. M. Kennedy acknowledges funding from the fast start Marsden Fund (09-UO-017C); and the International Science and Technology (ISAT) Linkages Fund (in New-Zealand) for an international co-operation grant with Germany, Y. Lavallée thanks the European Research Council Starting Grant on Strain Localisation in Magmas (SLiM, 306488).

## References

Arakeri JH, Avila FE, Dada JM, Tovar RO (2000) Convection in a long vertical tube due to unstable stratification-A new type of turbulent flow? Current Science 79(6):859-866

Bizouard H, Barberi F, Varet J (1980) Mineralogy and petrology of Erta Ale and Boina volcanic series, Afar rift, Ethiopia. Journal of Petrology 21(2):401-436

Cimarelli C, Di Traglia F, Taddeucci J (2010) Basaltic scoria textures from a zoned conduit as precursors to violent Strombolian activity. Geology 38(5):439-442

Clemente CS, Amorós EB, Crespo MG (2007) Dike intrusion under shear stress: effects on magnetic and vesicle fabrics in dikes from rift zones of Tenerife (Canary Islands). Journal of Structural Geology 29(12):1931-1942

Cole J, Cashman K, Rankin P (1983) Rare-earth element geochemistry and the origin of andesites and basalts of the Taupo Volcanic Zone, New Zealand. Chemical geology 38(3):255-274

Coward MP (1980) The analysis of flow profiles in a basaltic dyke using strained vesicles. J. Geol. Soc. 137(SEP):605-615

Debacq M, Hulin J-P, Salin D, Perrin B, Hinch EJ (2003) Buoyant mixing of miscible fluids of varying viscosities in vertical tubes. Physics of Fluids 15(12):3846-3855

Demant A, Lestrade P, Lubala RT, Kampunzu AB, Durieux J (1994) Volcanological and petrological evolution of Nyiragongo volcano, Virunga volcanic field, Zaire. Bull Volcanol 56(1):47-61

Dibble RR, Kienle J, Kyle PR, Shibuya K (1984) Geophysical studies of Erebus volcano, Antarctica, from 1974 December to 1982 January. N. Z. J. Geol. Geophys. 27(4):425-455

Fitzgerald R, Tsunematsu K, Kennedy B, Breard E, Lube G, Wilson T, Jolly A, Pawson J, Rosenberg M, Cronin S (2014) The application of a calibrated 3D ballistic trajectory model to ballistic hazard assessments at Upper Te Maari, Tongariro. Journal of Volcanology and Geothermal Research 286:248-262

Garcia MO, Pietruszka AJ, Rhodes JM, Swanson K (2000) Magmatic processes during the prolonged Pu'u'O'o eruption of Kilauea Volcano, Hawaii. Journal of Petrology 41(7):967-990

Genareau K, Valentine G, Moore G, Hervig R (2010) Mechanisms for transition in eruptive style at a monogenetic scoria cone revealed by microtextural analyses (Lathrop Wells volcano, Nevada, U.S.A.). Bull Volcanol 72(5):593-607

Geshi N, Kusumoto S, Gudmundsson A (2010) Geometric difference between non-feeder and feeder dikes. Geology 38(3):195-198

Geshi N, Neri M (2014) Dynamic feeder dyke systems in basaltic volcanoes: the exceptional example of the 1809 Etna eruption (Italy). Frontiers in Earth Science 2:13

Giberti G, Jaupart C, Sartoris G (1992) Steady-state operation of Stromboli volcano, Italy: constraints on the feeding system. Bull Volcanol 54(7):535-541

Gonnermann HM, Manga M (2007) The Fluid Mechanics Inside a Volcano. Annual Review of Fluid Mechanics 39(1):321-356

Harris AJL, Carniel R, Jones J (2005) Identification of variable convective regimes at Erta Ale Lava Lake. Journal of Volcanology and Geothermal Research 142(3–4):207-223

Heliker C, Wright TL (1991) The Pu'u 'O'o-Kupaianaha Eruption of Kilauea. Eos, Transactions American Geophysical Union 72(47):521-530

Hobden B (1997) Modelling magmatic trends in time and space: Eruptive and magmatic history of the Tongariro Volcanic Complex, New Zealand.

Hobden B, Houghton B, Davidson J, Weaver S (1999) Small and short-lived magma batches at composite volcanoes: time windows at Tongariro volcano, New Zealand. J. Geol. Soc. 156(5):865-868

Huppert HE, Hallworth MA (2007) Bi-directional flows in constrained systems. Journal of Fluid Mechanics 578:95-112

Jaupart C, Vergniolle S (1989) The generation and collapse of a foam layer at the roof of a basaltic magma chamber. Journal of Fluid Mechanics 203:347-380

Keating GN, Valentine GA, Krier DJ, Perry FV (2008) Shallow plumbing systems for small-volume basaltic volcanoes. Bulletin of Volcanology 70(5):563-582

Laiolo M, Cigolini C (2006) Mafic and ultramafic xenoliths in San Bartolo lava field: New insights on the ascent and storage of Stromboli magmas. Bull Volcanol 68(7-8):653-670

Lautze NC, Houghton BF (2005) Physical mingling of magma and complex eruption dynamics in the shallow conduit at Stromboli volcano, Italy. Geology 33(5):425-428

Lautze NC, Houghton BF (2007) Linking variable explosion style and magma textures during 2002 at Stromboli volcano, Italy. Bull Volcanol 69(4):445-460

Lefebvre NS, White JDL, Kjarsgaard, BA (2012) Spatter-dike reveals subterranean magma diversions: Consequences for samll multivent basaltic eruptions. Geology 40:423-426

Llewellin E, Del Bello E, Taddeucci J, Scarlato P, Lane S (2012) The thickness of the falling film of liquid around a Taylor bubble. Proceedings of the Royal Society A: Mathematical, Physical and Engineering Science 468(2140):1041-1064

McArthur JL, Shepherd MJ (1990) Late Quaternary glaciation of Mt Ruapehu, North Island, New Zealand. Journal of the Royal Society of New Zealand 20(3):287-296

Miles JW (1959) On the generation of surface waves by shear flows Part 3. Kelvin-Helmholtz instability. Journal of Fluid Mechanics 6(04):583-598

Moebis A, Cronin SJ, Neall VE, Smith IE (2011) Unravelling a complex volcanic history from fine-grained, intricate Holocene ash sequences at the Tongariro Volcanic Centre, New Zealand. Quaternary International 246(1):352-363

Nairn IA, Kobayashi T, Nakagawa M (1998) The similar to 10 ka multiple vent pyroclastic eruption sequence at Tongariro Volcanic Centre, Taupo Volcanic Zone, New Zealand: Part 1. Eruptive processes during regional extension. Journal of Volcanology and Geothermal Research 86(1-4):19-44

Oppenheimer C, Kyle PR (2008) Probing the magma plumbing of Erebus volcano, Antarctica, by open-path FTIR spectroscopy of gas emissions. Journal of Volcanology and Geothermal Research 177(3):743-754

Palma JL, Blake S, Calder ES (2011) Constraints on the rates of degassing and convection in basaltic open-vent volcanoes. Geochemistry, Geophysics, Geosystems 12(11):Q11006

Parfitt E, Wilson L (1995) Explosive volcanic eruptions—IX. The transition between Hawaiian-style lava fountaining and Strombolian explosive activity. Geophysical Journal International 121(1):226-232

Parfitt EA (2004) A discussion of the mechanisms of explosive basaltic eruptions. Journal of Volcanology and Geothermal Research 134(1):77-107

Philpotts AR, Philpotts DE (2007) Upward and downward flow in a camptonite dike as recorded by deformed vesicles and the anisotropy of magnetic susceptibility (AMS). Journal of Volcanology and Geothermal Research 161(1-2):81-94

Rust A, Manga M (2002) Bubble shapes and orientations in low Re simple shear flow. Journal of colloid and interface science 249(2):476-480

Rust AC, Manga M, Cashman KV (2003) Determining flow type, shear rate and shear stress in magmas from bubble shapes and orientations. Journal of Volcanology and Geothermal Research 122(1–2):111-132

Stevens NF (2002) Emplacement of the large andesite lava flow in the Oturere Stream valley, Tongariro Volcano, from airborne interferometric radar. N. Z. J. Geol. Geophys. 45(3):387-394

480 Stevenson DS, Blake S (1998) Modelling the dynamics and thermodynamics of volcanic degassing.
481 Bull Volcanol 60(4):307-317
482
483 Stovall WK, Houghton BF, Harris AJL, Swanson DA (2009) A frozen record of density-driven crustal
484 overturn in lava lakes: the example of K&Aumlaut << lauea Iki 1959. Bull Volcanol 71(3):313-318
485
486 Taisne B, Jaupart C (2009) Dike propagation through layered rocks. J. Geophys. Res.-Solid Earth 114
487
488 Watanabe H, Okubo S, Sakashita S, Maekawa T (1998) Drain-back process of basaltic magma in the
489 summit conduit detected by microgravity observation at Izu-Oshima volcano, Japan. Geophysical
490 Research Letters 25(15):2865-2868
491
492 Witham F, Llewellin EW (2006) Stability of lava lakes. Journal of Volcanology and Geothermal
493 Research 158(3–4):321-332
494
495 Witham F, Woods A, Gladstone C (2006) An analogue experimental model of depth fluctuations in
496 lava lakes. Bull Volcanol 69(1):51-56
497
498 Witter JB, Kress VC, Delmelle P, Stix J (2004) Volatile degassing, petrology, and magma dynamics of
499 the Villarrica Lava Lake, Southern Chile. Journal of Volcanology and Geothermal Research 134(4):303-
500 337
501
502

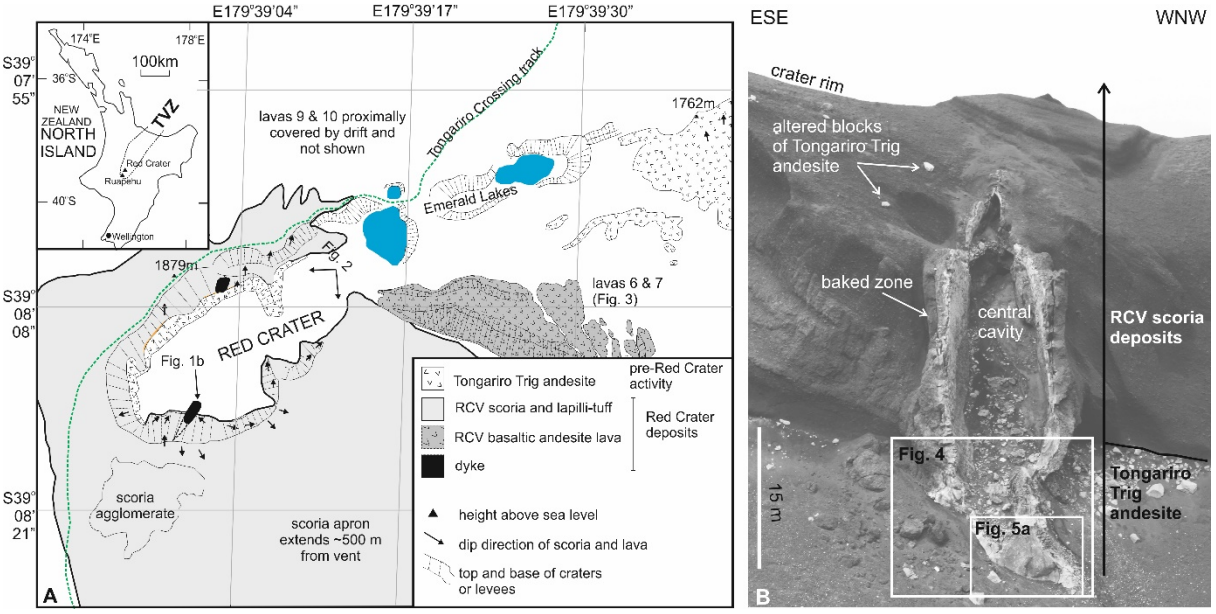


**Figure 1**

A – simplified geological map of Red Crater vent in the Tongariro Volcanic Centre, New Zealand, showing the exposure of the Tongariro Trig andesite, Red Crater volcano basaltic andesite lavas 6 and 7 (lava emplacement sequence of Topping, 1973) and the Red Crater scoria cone and dykes in the Oturere Valley. Inset: Red Crater location in New Zealand. B – photograph of the ~45 m high dyke exposure showing the exposed dyke-conduit geometry.

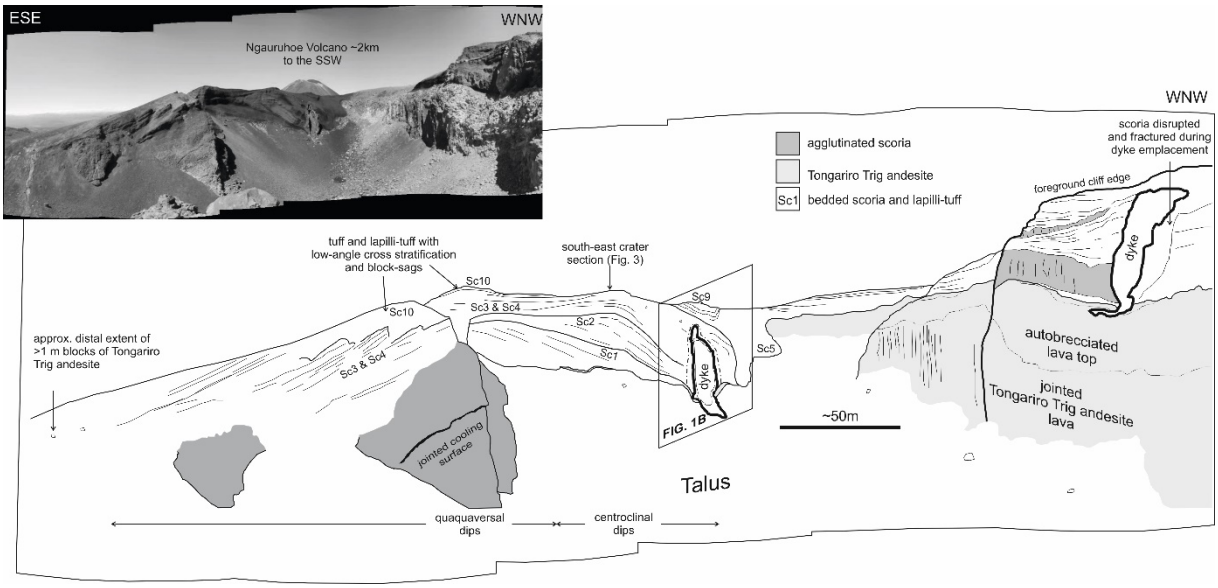


**Figure 2**

Annotated field sketch of an oblique, SW-facing view of the proximal area of the Red Crater volcano showing the interior walls of the scoria cone with locally agglutinated beds and the position of the dykes preserved in the south and north crater walls. Photograph of the same view is provided for comparison.

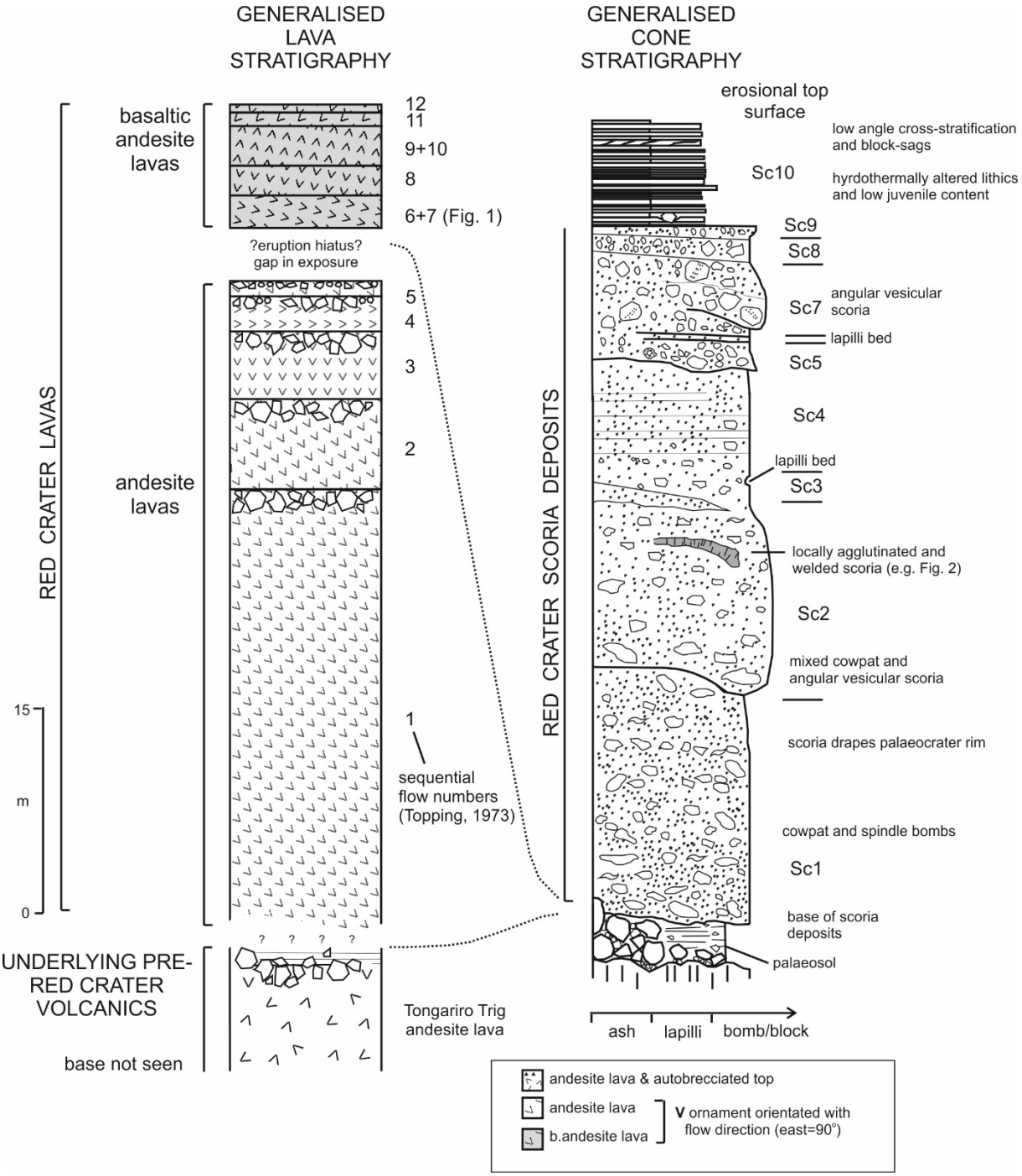


**Figure 3**

Stratigraphic section through the Red Crater volcano lavas and the Red Crater volcano proximal scoria deposits showing the textural evolution of the eruptive products. We note the lowermost portion of the section is dominated by flattened clasts and local agglutination (Sc1-4), in contrast with the overlying portion of more equant clasts with no evidence for agglutination (Sc5-9). Overlying the scoria deposits are fine grained, finely bedded lapilli-tuff and tuff (Sc10).

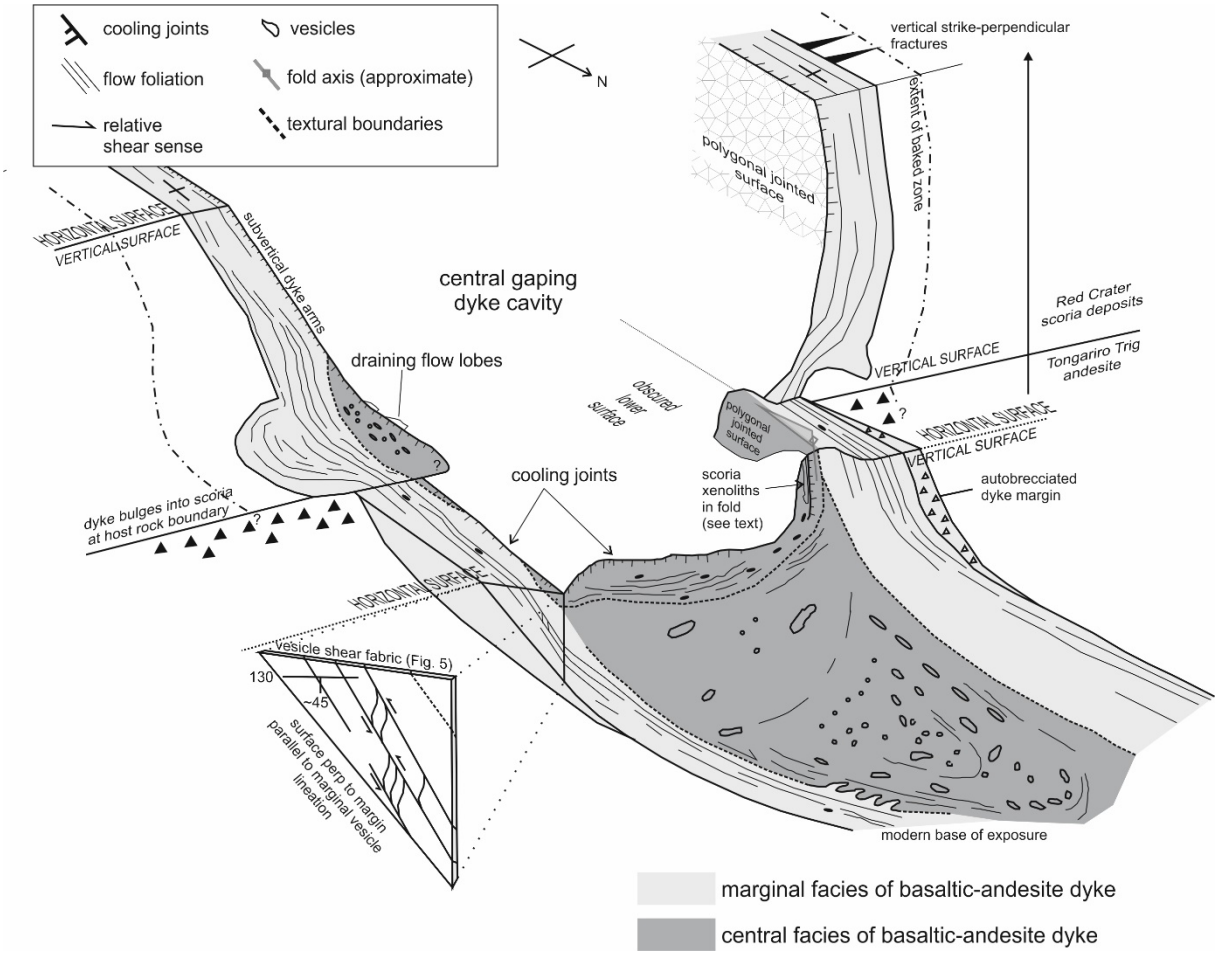


**Figure 4**

Sketch of the lower portion of the dyke preserved in the south interior wall of the Red Crater volcano scoria deposits. Schematically summarised are the main features of the dyke referred to in the text.

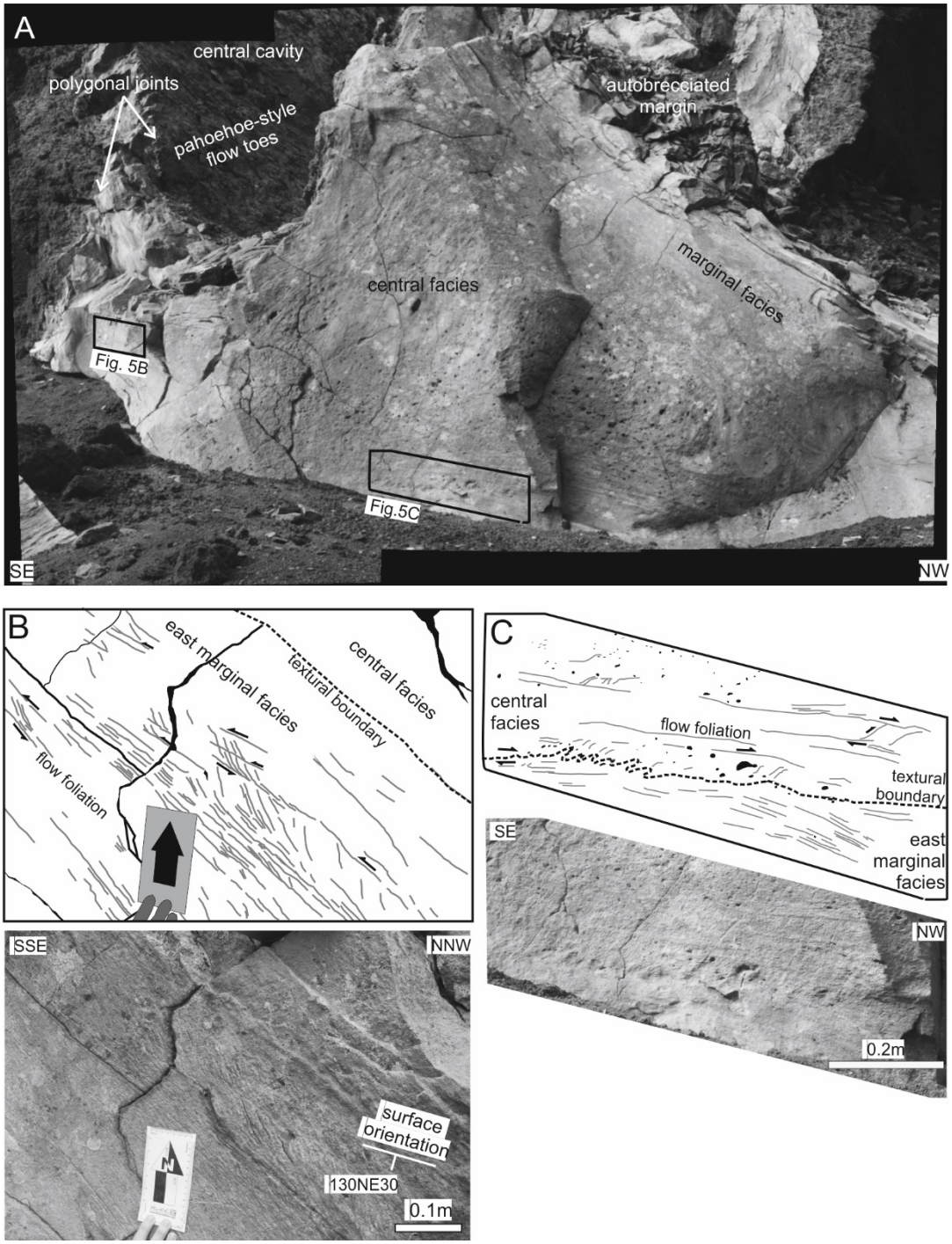


528

529 **Figure 5**

530 Field photographs and sketches showing kinematic detail used to infer magma flow directions. A – an
531 overview photograph of the lower part of the dyke exposure. B – near the contact between the
532 marginal facies and the central facies showing kinematic ductile shear fabric recording upward relative
533 movement within the marginal zones – arrows depict relative shear sense. C – contact between the
534 marginal facies and the central facies showing asymmetrical, west-verging folded margin, and shear
535 fabric recording downward relative motion of the central facies.

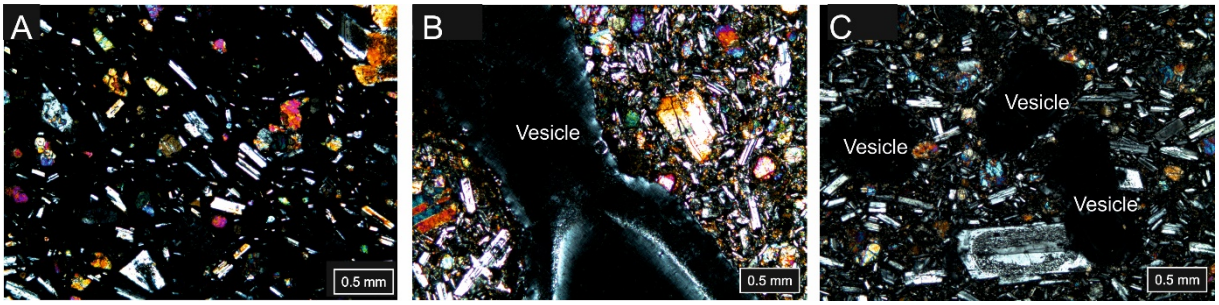


**Figure 6**

Photomicrographs taken in cross-polarised transmitted light of thin sections from (A) the marginal facies, (B) the central facies and (C) the uppermost surface of the central facies.

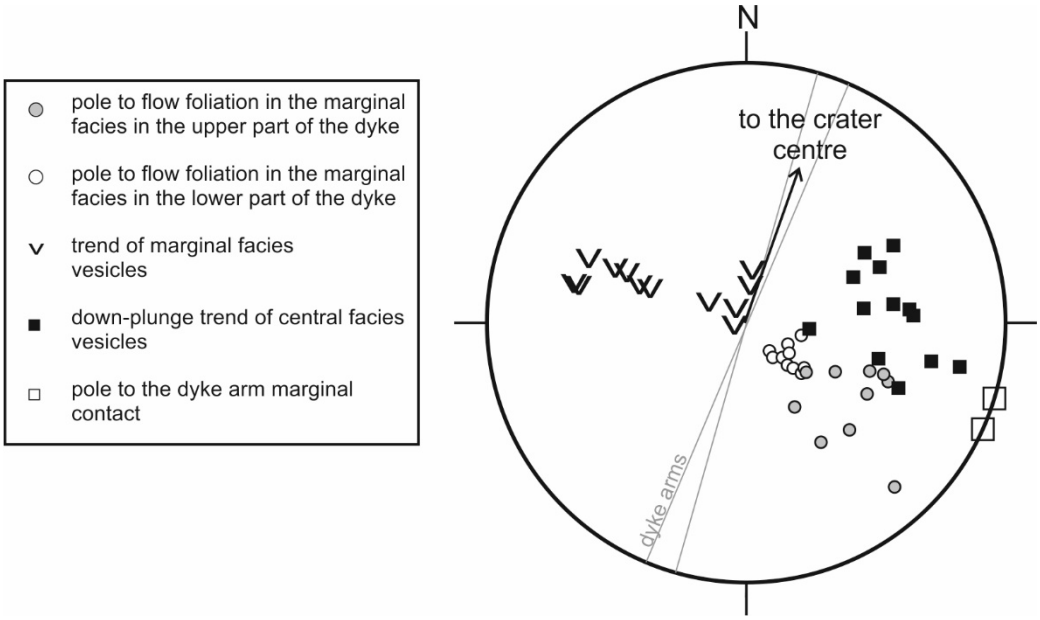


**Figure 7**

Lower hemisphere projection of structural data showing the upper (near-vertical) portions of the dyke arms as great circles and poles to the planes of planar features such as flow foliation and trend-plunge data for linear features such as vesicle orientations presented as single points. All vesicle and flow foliation data are taken on the east side of the dyke so that they can be directly compared.